BIOCHEMISTRY
including biophysical chemistry & molecular biology
Article

Biochemistry **2010,** *49,* 601–610 601
DOI: 10.1021/bi901579y

Efavirenz Binding to HIV-1 Reverse Transcriptase Monomers and Dimers[†]

Valerie A. Braz, Leslie A. Holladay,[‡] and Mary D. Barkley*

Department of Chemistry, Case Western Reserve University, 10900 Euclid Avenue, Cleveland, Ohio 44106. [‡]*Mailing address: P.O. Box 244, Townsend, TN 37882. E-mail: holladayl@aol.com.*

Received September 9, 2009; Revised Manuscript Received November 4, 2009

ABSTRACT: Efavirenz (EFV) is a nonnucleoside reverse transcriptase inhibitor (NNRTI) of HIV-1 reverse transcriptase (RT) used for the treatment of AIDS. RT is a heterodimer composed of p66 and p51 subunits; p51 is produced from p66 by C-terminal truncation by HIV protease. The monomers can form p66/p66 and p51/p51 homodimers as well as the p66/p51 heterodimer. Dimerization and efavirenz binding are coupled processes. In the crystal structure of the p66/p51−EFV complex, the drug is bound to the p66 subunit. The binding of efavirenz to wild-type and dimerization-defective RT proteins was studied by equilibrium dialysis, tryptophan fluorescence, and native gel electrophoresis. A 1:1 binding stoichiometry was determined for both monomers and homodimers. Equilibrium dissociation constants are ~2.5 μM for both p66− and p51−EFV complexes, 250 nM for the p66/p66−EFV complex, and 7 nM for the p51/p51−EFV complex. An equilibrium dissociation constant of 92 nM for the p66/p51−EFV complex was calculated from the thermodynamic linkage between dimerization and inhibitor binding. Binding and unbinding kinetics monitored by fluorescence were slow. Progress curve analyses revealed a one-step, direct binding mechanism with association rate constants k_1 of ~13.5 M^{-1} s^{-1} for monomers and heterodimer and dissociation rate constants k_{-1} of ~9 × 10^{-5} s^{-1} for monomers. A conformational selection mechanism is proposed to account for the slow association rate. These results show that efavirenz is a slow, tight-binding inhibitor capable of binding all forms of RT and suggest that the NNRTI binding site in monomers and dimers is similar.

HIV-1[1] RT converts single-stranded viral RNA into double-stranded proviral DNA. The enzyme has two activities, DNA polymerase and RNase H. The biologically relevant form is a heterodimer composed of two subunits, p66 and p51 (*1*). The subunits are products of the same gene and have identical N-terminal amino acid sequences; p51 lacks the C-terminal RNase H domain (*2*−*4*). The individual subunits can also form homodimers. The p66 subunit in the heterodimer has both polymerase and RNase H active sites (*5*). The monomeric species are devoid of enzymatic activity (*3*, *4*). Because of its essential role in the HIV life cycle, RT is a major target of antiretroviral drugs (*6*). Two classes of inhibitors have been developed and approved for clinical use, NRTIs and NNRTIs. The NNRTIs are highly effective and relatively noncytotoxic (*7*). These small, amphiphilic, noncompetitive inhibitors nestle into a hydrophobic pocket ~10 Å from the polymerase active site in the p66 subunit of RT (*8*, *9*). NNRTIs primarily interfere with reverse transcription, but they also affect late stages of HIV replication in Gag-Pol polyprotein processing (*10*−*12*).

NNRTIs have diverse effects on RT subunit dimerization. Efavirenz (EFV) and nevirapine (NVP) enhance subunit interactions (*13*, *14*); delavirdine has little or no effect (*13*), and TSAOe[3]T, BBNH, and BBSH weaken subunit interactions (*15*, *16*). The evidence for these results derives from multiple techniques, including yeast two-hybrid, pull-down assays, urea-induced dissociation, size exclusion chromatography, and sedimentation equilibrium studies. To explain the contrasting effects of NNRTI binding on RT, we previously proposed a thermodynamic cycle (*14*). In Scheme 1, P denotes p66 or p51 monomer, P/P is p66/p51 heterodimer, p66/p66 homodimer, or p51/p51 homodimer, and I is NNRTI. The thermodynamic linkage between NNRTI binding and RT subunit dimerization makes the following predictions. (1) NNRTIs bind to both monomeric and dimeric forms of RT proteins. The crystal structures of RT−NNRTI complexes show one drug bound per heterodimer (*8*, *9*). In solution, the stoichiometry of drug binding to the dimer is not known. (2) NNRTIs that enhance dimerization bind more tightly to dimers. Conversely, NNRTIs that weaken dimerization bind more tightly to monomers. Identifying and quantifying the various protein−ligand interactions are essential for a thorough understanding of the inhibition mechanism of NNRTIs. The previous thermodynamic cycle (Scheme 1 in ref *14*) makes the additional prediction that low concentrations of inhibitor will

[†]This work was supported by National Institutes of Health Grant GM071267.

*To whom correspondence should be addressed. Telephone: (216) 368-0602. Fax: (216) 368-0604. E-mail: mdb4@case.edu.

[1]Abbreviations: BBNH, *N*-(4-*tert*-butylbenzoyl)-2-hydroxy-1-naphthaldehyde hydrazone; BBSH, (4-*tert*-butylbenzoyl)-2-hydroxy-1-salicylyl hydrazone; BN-PAGE, Blue Native polyacrylamide gel electrophoresis; DMF, dimethylformamide; DMSO, dimethyl sulfoxide; EDTA, ethylenediaminetetraacetic acid; EFV, efavirenz; HIV-1, human immunodeficiency virus type 1; ITC, isothermal titration calorimetry; NATA, *N*-acetyltryptophanamide; Ni-NTA, nitriloacetic acid; NNRTI, nonnucleoside reverse transcriptase inhibitor; NRTI, nucleoside reverse transcriptase inhibitor; NVP, nevirapine; PDB, Protein Data Bank; PR, HIV-1 protease; RT, reverse transcriptase; SPR, surface plasmon resonance; Tris, tris(hydroxymethyl)aminomethane; TCEP, tris(2-carboxyethyl)phosphine; TSAOe3T, 1-(spiro{4″-amino-2″,2″-dioxo-1″,2″-oxathiole-5″,3′-[2′,5′-bis-*O*-(*tert*-butyldimethylsilyl)-*β*-D-ribofuranosyl]})-3-ethylthymine.

Published on Web 12/29/2009

Scheme 1: Thermodynamic Linkage of NNRTI Binding and Subunit Dimerization

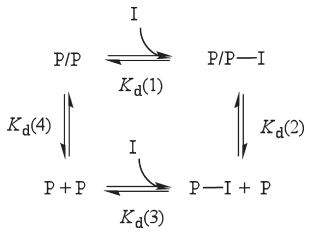

promote dimerization if $K_d(1) < K_d(3)$.[2] However, eventually Le Châtelier's principle will shift the equilibrium toward the formation of P−I at high concentrations of inhibitor.

Previous sedimentation equilibrium studies showed that efavirenz enhances the formation of p66/p51, p66/p66, and p51/p51 by 25-, 50-, and 600-fold, respectively (*14*). Here we assess the binding of efavirenz to p66 and p51 monomers in wild-type and dimerization-defective mutant RTs and determine the binding stoichiometry of monomers and homodimers. Binding stoichiometry and equilibrium dissociation constants for binding of drug to dimer and monomer, $K_d(1)$ and $K_d(3)$, respectively, were determined by equilibrium dialysis. The kinetics of binding of drug to monomers and heterodimer were monitored by intrinsic protein fluorescence. Finally, the binding of [^{14}C]efavirenz to p66 monomer and p66/p66 homodimer was visualized by Blue Native gel electrophoresis.

EXPERIMENTAL PROCEDURES

Materials. Efavirenz was obtained from the NIH AIDS Research and Reference Reagent Program (Germantown, MD). [^{14}C]Efavirenz (specific activity of 52 mCi/mmol) was purchased from Vitrax (Placentia, CA). Dialysis tubing was purchased from Spectrum Laboratories (Rancho Dominguez, CA). Rapid equilibrium dialysis (RED) devices and TCEP were purchased from Pierce (Rockford, IL). Econo-Safe scintillation fluid was purchased from Atlantic Nuclear Corp. (Canton, MA). Oligodeoxynucleotide primers, 5% Coomassie blue G-250 sample additive, and NativePAGE Novex Bis-Tris gel systems were purchased from Invitrogen Corp. (Carlsbad, CA). EZ-Run Protein Gel Staining solution was purchased from Fisher Scientific (Fair Lawn, NJ). Biochemical reagents were purchased from Roche Applied Science (Indianapolis, IN). Other chemicals were from Sigma Chemicals (St. Louis, MO). RT buffer D consists of 0.05 M Tris (pH 7.0), 25 mM NaCl, 1 mM EDTA, and 10% (v/v) glycerol (molecular biology grade redistilled).

Protein Preparation. HIV-1 RT proteins with N-terminal hexahistidine extensions were expressed in *Escherichia coli* M15 strains containing plasmid p6H RT for p66, p6H RT51 for p51, or p6H RT-PR for p66/p51 heterodimer and purified by Ni-NTA, S-Sepharose, and DEAE chromatography as previously described (*14*, *17*). The protein concentration is determined from the absorbance at 280 nm and is expressed in monomer units (*14*, *18*). Protein stock solutions were dialyzed overnight into RT buffer D containing 1 mM TCEP[3] prior to use.

Dimerization-defective RT proteins were prepared from plasmids p6H RT and p6H RT51 containing the W401A mutation (*19*). The W401A mutation was introduced by one round of mutagenesis using the QuickChange site-directed mutagenesis kit (Stratagene, La Jolla, CA). The oligonucleotide primer sequences were as follows: forward, 5′-GGGAAACA-GCGTGGCCAGAGTATTGGCAAGCCACCTG-3′; reverse, 5′-CAGGTGGCTTGCCAATACTCTGTCCACGCTGTTT-CCC-3′. All mutations were confirmed by DNA sequencing at Agencourt Bioscience (Beverly, MA).

Equilibrium Dialysis. Equilibrium dialysis experiments were conducted using 1.5 mL RNase/DNase free amber microcentrifuge tubes and 4 mm dialysis tubing with 3500 molecular weight cutoff or RED devices. A 1 mM stock solution of [^{14}C]efavirenz in DMF was prepared. A 250 μL aliquot of the RT solution was loaded into dialysis tubing or one chamber of the RED device. RT concentrations were 0.1−10 μM p51, 1−10 μM p51^{W401A}, 2−4 μM p51^{L234A}, 0.4−5 μM p66, and 0.8−7.5 μM p66^{W401A}. RT buffer D containing 1 mM TCEP and 0.2−20 μM [^{14}C]-efavirenz was used as dialysate buffer. For microcentrifuge tubes, the dialysis bag and 1 mL of dialysate buffer were placed in the tube and the tube was capped. For RED devices, 0.4 mL of dialysate buffer was placed in the other chamber. The samples were set up in triplicate, secured to a benchtop rotator, and dialyzed at 4 °C. Wild-type RT proteins were dialyzed for up to 5 days; W401A mutant proteins were dialyzed for 30 h. Equilibration of efavirenz across the membrane occurred by 20 h.

Efavirenz binding was quantified by counting three 50 μL aliquots of the inside protein solution and outside dialysate solution in 5 mL of scintillation fluid using a Beckman Coulter LS6500 multipurpose scintillation counter. A buffer blank and 50 μL aliquots of the initial dialysate solution were also counted. The bound ligand concentration was calculated from

$$[I_{bound}] = [I_{in}] - [I_{out}] \quad (1)$$

where $[I_{in}]$ is the total concentration of free and bound efavirenz inside the dialysis tubing or RED chamber and $[I_{out}] = [I]$ is the concentration of free efavirenz in the outside dialysate. Scintillation counting data were converted to molarity and fit to mathematical models in the Dialfit program as described in the Appendix. The value of $K_a(4)$ was fixed in the data analysis using a ln K_a value of 8.3 for the p51/p51 homodimer and a ln K_a value of 12.4 for the p66/p66 homodimer (*14*).

Isothermal Titration Calorimetry. ITC experiments were performed on a Microcal VP-ITC microcalorimeter. Wild-type p51 solutions (1.5 and 3.0 μM) were titrated with efavirenz (200 μM) in RT buffer D containing 3% DMF at 5 °C. Prior to the reaction, p51 was dialyzed into RT buffer D containing 3% DMF to eliminate any solvent effects. Aliquots of 5, 10, and 15 μL of the efavirenz solution were added over 60 min to a final concentration of 40 μM. The amounts of heat released after each addition of efavirenz into the p51 solution and the buffer blank were identical, indicating that (1) the binding event is too slow to measure by this technique or (2) $\Delta H = 0$.

Fluorescence. Absorbance was measured on a Cary 3E UV−vis spectrophotometer. Fluorescence was measured on a PC1 photon counting spectrofluorometer (ISS, Champaign, IL) in ratio mode under magic angle conditions using 4 nm excitation and 16 nm emission bandwidths at 5 °C. The sample compartment was flushed with nitrogen to prevent condensation. Samples were placed in 45 μL quartz cells with a path length of 3 mm (Starna Cells, Inc., Atascadero, CA). Absorbance at 280 nm was < 0.3 to avoid inner filter effects. Fluorescence quantum yields Φ were measured at an excitation wavelength of 295 nm relative to

[2] In the previous thermodynamic cycle, reaction 2 for dimerization in the presence of NNRTI is written as P/P−I + I = 2P−I. The dissociation constant for this reaction is a composite equilibrium constant equal to $K_d(2)/K_d(3)$.

[3] Addition of 1 mM TCEP to RT buffer D lowered the pH from 7.0 to 6.5.

NATA in water with a Φ of 0.23 at 5 °C. The quantum yield of NATA at 5 °C was determined relative to tryptophan in water at an excitation wavelength of 295 nm and 25 °C, with a Φ of 0.14 (*20*).

Association and dissociation kinetics of RT proteins and efavirenz were monitored by fluorescence using Vinci 1.6.SP7 (ISS). The intrinsic tryptophan fluorescence was measured at an excitation wavelength of 295 nm and an emission wavelength of 340 nm using NATA in water as a reference. Slow kinetic intensity data were collected from samples and NATA every 30 s (signal averaged over 5 s) for 4−5 h, and then every 5 min (signal averaged over 10 s) for 27 h. Fluorescence intensity $F = I_s/I_r$ was calculated from the ratio of sample intensity I_s to reference intensity I_r to correct for instrumental drift.

Association reactions were started via addition of 2 μL of a diluted efavirenz stock solution (250 mM in DMF) to 80 μL of 2.5 μM $p66^{W401A}$ or $p51^{W401A}$, 4.5 μM wild-type p51, or 10-fold dilution of 20 μM p66/p51 (85% dimer). The solution was mixed in the cell for 5 s and immediately placed in the fluorometer. Final efavirenz concentrations were 4−40 μM. Dissociation reactions were started by 100-fold dilution of 20 μM $p66^{W401A}$ or $p51^{W401A}$ equilibrated with 35 μM efavirenz. The change in intrinsic tryptophan fluorescence due to binding or unbinding of efavirenz was fit to a single-exponential function.

$$[F(t) - F_0]/(F_\infty - F_0) = C[1 - \exp(-k_{obs}t)] \quad (2a)$$

$$[F(t) - F_\infty]/(F_0 - F_\infty) = C_1 \exp(-k_{diss}t) + C_2 \quad (2b)$$

where $F(t)$ is the intensity at time t, F_0 is the intensity at time zero, F_∞ is the intensity of the last time point, and the C terms are constants.

Native Gel Electrophoresis. BN-PAGE was conducted using the Novex Bis-Tris gel system as described previously (*21*). A 5−10 μL aliquot of 2 μM $p66^{W401A}$ and 0.8−5 μM p66 in the absence or presence of NNRTI was mixed with 0.3 μL of Coomassie G-250 sample additive, 2.5 μL of NativePAGE Sample Buffer, and water to a final volume of 15 μL. Gels were stained with EZ-Run Protein Gel Staining solution and destained in water. For gels containing [^{14}C]efavirenz, p66 was incubated for 2 h or 1 week and subjected to BN-PAGE. Gels were imaged by a PhosphorImager (Amersham Biosciences, Piscataway, NJ), viewed with ImageQuant, and then stained in EZ-Run Protein Gel Staining solution and destained in water.

RESULTS

Equilibrium Dialysis. Binding of efavirenz to p66 and p51 is coupled to formation of homo- and heterodimers (Scheme 1). Dimerization constants in the absence and presence of NNRTI are characterized by $K_d(4)$ and $K_d(2)$, while inhibitor dissociation constants of dimer and monomer complexes are $K_d(1)$ and $K_d(3)$. Dimerization constants for p66/p66 and p51/p51 homodimers in the absence and presence of efavirenz were previously determined by sedimentation equilibrium (*14*). Equilibrium dialysis was used to determine inhibitor dissociation constants $K_d(1)$ and $K_d(3)$.

Equilibrium binding experiments were initially set up with p51, because the dimerization constants in the absence and presence of efavirenz, $K_d(4) = 230$ μM for p51/p51, and $K_d(2) = 0.37$ μM for the p51/p51−I complex, respectively, provide access to both monomer and homodimer. The first binding experiments used 10 μM p51 (7.5% homodimer) and 20 μM [^{14}C]efavirenz. Dialysis was terminated, and samples were analyzed at 30 h and at 3, 5, and 7 days. After 30 h, the ratio of efavirenz to p51 was ~0.84:1, indicating a binding stoichiometry of either one inhibitor per p51 monomer or two inhibitors per p51/p51 homodimer. The ratio of efavirenz to p51 decreased to 0.68:1 after 3 days, 0.52:1 after 5 days, and 0.49:1 after 7 days. A ratio of one efavirenz per p51/p51 homodimer is consistent with the stoichiometry in the crystal structure of the p66/p51−EFV complex (*9*). Because of the slow dimerization, all experiments examining binding of efavirenz to dimeric species were equilibrated for 5 days. To confirm that the 30 h dialysis with wild-type p51 represents efavirenz binding to monomer, equilibrium dialysis experiments were also performed using dimerization-defective RT proteins. Two dimerization-defective mutations reported in the literature are L234A (*22*, *23*) and W401A (*19*). L234A is a primer grip mutation; W401A is a mutation in the tryptophan repeat motif of the connection subdomain. The presence of either of these mutations in the p66 or p51 subunit of the heterodimer results in dimerization deficiency, the mutation in p66 having the most detrimental effect. Equilibrium dialysis experiments set up with 3−6 μM $p51^{L234A}$ and 5−12 μM [^{14}C]efavirenz failed to detect any bound efavirenz. Thus, the L234A mutation prevents not only dimerization but also efavirenz binding. This is not surprising given that L234 is a contact residue in the NNRTI binding pocket.

Inhibitor dissociation constants $K_d(1)$ and $K_d(3)$ were determined by simultaneously varying protein and efavirenz concentrations in equilibrium dialysis experiments. The data sets for multiple concentrations of protein and efavirenz were analyzed with Dialfit (Appendix). The ln $K_a(4)$ value, where $K_a(4)$ is the equilibrium association constant of the p51/p51 or p66/p66 homodimer (*14*), is set as a constant, and ln K_a values for binding of the inhibitor to monomers and dimers are allowed to float. Data sets for wild-type RT proteins equilibrated with efavirenz were fit to the coupled equilibria in Scheme 1; data sets for the dimerization-defective mutants were fit neglecting the dimerization reaction. Weighted least-squares fits were performed until the fits converged. Figure 1A shows efavirenz binding data for wild-type p51 together with the fit to eqs A1a−A1c for the coupled equilibria. The $\log[I_{bound}]$ is plotted for the sake of clarity; $[I_{bound}]$ in micromolar was used in the data analysis. To illustrate the range of efavirenz and protein concentrations used in the experiments, the residuals $[I_{bound}]_{exp} - [I_{bound}]_{calc}$ are plotted versus the total protein concentration (inset). Figure 1B shows efavirenz binding data for $p51^{W401A}$ and the fit to eq A1a for a simple binding equilibrium.

Table 1 gives the results of the global analyses for wild-type and dimerization-defective RT proteins. Dissociation constants $K_d(1)$ and $K_d(3)$ for binding of efavirenz to dimers and monomers were calculated from K_a values with the relationship $K_d = 1/K_a$. The inhibitor dissociation constant $K_d(1)$ of wild-type homodimer−EFV complexes is ~36-fold tighter for the p51/p51−EFV complex than for the p66/p66−EFV complex: K_d(p51/p51−I) = 7 nM compared to K_d(p66/p66−I) = 250 nM. The inhibitor dissociation constants $K_d(3)$ of wild-type and dimerization-defective monomer−EFV complexes are much weaker, in the micromolar range. The $K_d(3)$ values for wild-type p66 and p51 measured after equilibration with efavirenz for 5 days are inaccurate. At high protein concentrations, the free monomer concentration is too low to detect, and at low protein concentrations, binding of efavirenz to the monomer is too weak to detect. The data set for wild-type p51 equilibrated for 30 h with efavirenz provides a more reliable value for $K_d(3)$ of 1.7 μM, because at 30 h wild-type p51 is ~70% monomer. The inhibitor dissociation

constants $K_d(3)$ for $p51^{W401A}$−EFV and $p66^{W401A}$−EFV complexes of 2.4−2.7 μM are within error of the value for wild-type p51, suggesting that the efavirenz binding site is the same in all the monomers.

Binding Kinetics. RT contains multiple tryptophan residues, 19 in p66 and 18 in p51 (Figure 2). Tryptophan fluorescence is exquisitely sensitive to the local electrostatic environment of the indole chromophore (*24*, *25*). Changes in RT fluorescence associated with dimerization and NNRTI binding have been reported previously (*26*, *27*). The fluorescence changes due to dimerization were attributed to the tryptophan repeat motif in the connection subdomain spanning residues 398−414. The NNRTI binding pocket contains β-sheet $\beta12-\beta13-\beta14$, which has two tryptophans, W229 and W239; W229 is in the loop between β-strands 12 and 13, and W239 is in β-strand 14. These two tryptophans may report conformational changes upon inhibitor binding.

The kinetics of binding of inhibitor to RT proteins were monitored by tryptophan fluorescence. Figure 3 shows that efavirenz binds slowly to p51 monomer and p66/p51 heterodimer. Approximately 50% of the overall fluorescence change occurs in ~2 h. To measure heterodimer fluorescence, a 20 μM solution containing 83% dimer was diluted 10-fold and efavirenz was added immediately to start the kinetics experiment before dissociation of the dimer occurs [$t_{1/2}$ = 2 days (*28*)]. The intensity

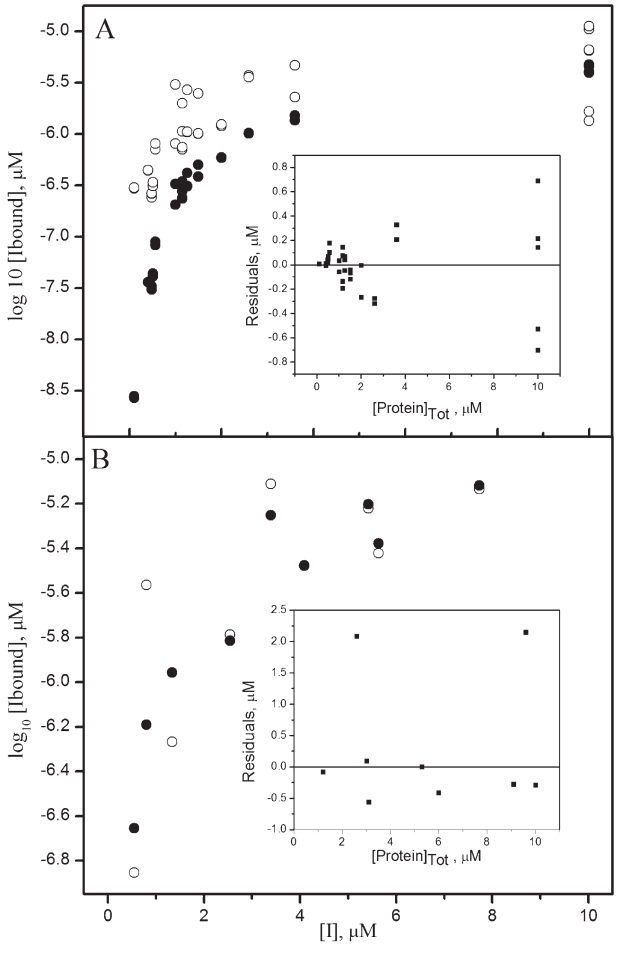

FIGURE 1: Equilibrium dialysis data for p51. (A) Wild-type p51 equilibrated with efavirenz for 5 days: (○) experimental values $[I_{bound}]_{exp}$ and (●) calculated values $[I_{bound}]_{calc}$ from Dialfit using eqs A1a−A1c. (B) $p51^{W401A}$ equilibrated with efavirenz for 30 h: (○) $[I_{bound}]_{exp}$ and (●) $[I_{bound}]_{calc}$ from Dialfit using eq A1a. Insets show residuals ($[I_{bound}]_{exp} - [I_{bound}]_{calc}$) vs total protein concentration $[Protein]_{Tot}$ in each measurement.

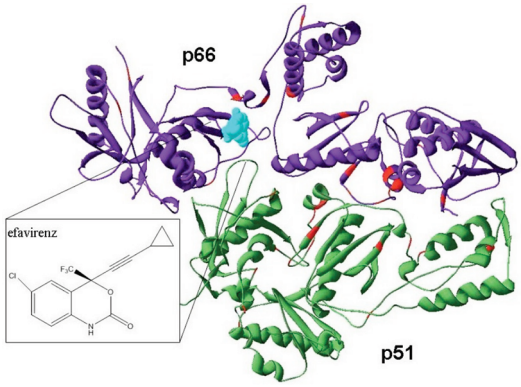

FIGURE 2: Structure of HIV-1 RT complexed with efavirenz (PDB entry 1FK9): p66 (purple), p51 (green), efavirenz (cyan), and tryptophans (red).

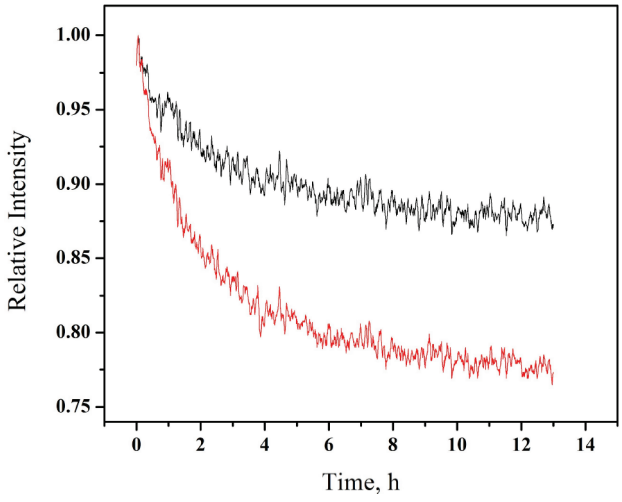

FIGURE 3: Association of efavirenz with (black line) p66/p51 and (red line) p51 monitored by tryptophan fluorescence at 5 °C. λ_{ex} = 295 nm, and λ_{em} = 340 nm. Twenty micromolar p66/p51 (83% heterodimer) diluted to 2 μM prior to addition of efavirenz; 4.5 μM p51 (97% monomer). EFV:protein concentration ratio of 2:1.

Table 1: Dissociation Constants[a]

protein	dialysis time	ln $K_a(1)$	$K_d(1)$ (μM)	ln $K_a(3)$	$K_d(3)$ (μM)
p51	30 h	17.3 ± 0.6	0.030 (0.017−0.056)	13.3 ± 0.6	1.7 (0.95−3.2)
p51	5 days	18.9 ± 0.8	0.0068 (0.0028−0.014)	10 ± 1	28 (10.1−75.0)
$p51^{W401A}$	30 h			12.9 ± 0.6	2.5 (1.3−4.4)
p66	5 days	15.2 ± 0.5	0.25 (0.15−0.41)	11 ± 1	19 (5.6−61)
$p66^{W401A}$	30 h			12.8 ± 0.3	2.7 (2.0−3.6)

[a]RT buffer D, 1 mM TCEP, at 5 °C. Global analysis of data sets for each protein and dialysis time from Dialfit. Errors in parentheses are 95% confidence intervals.

Scheme 2: Mechanisms of Slow Binding Inhibition

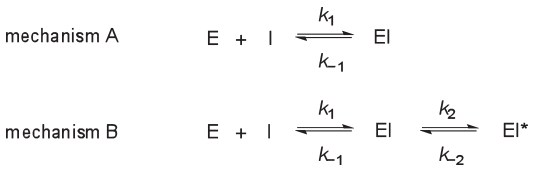

change for the heterodimer is approximately half that of the monomer, consistent with an effect on tryptophan residues in only one subunit.

Two kinetic mechanisms have been used to account for the slow binding of inhibitors to enzymes [Scheme 2 (*29*, *30*)]. Mechanism A depicts direct binding of inhibitor I to enzyme E, where the association and dissociation rate constants k_1 and k_{-1}, respectively, are inherently slow. Mechanism B depicts an induced-fit model with fast equilibration of inhibitor and enzyme to form an intermediate complex EI, followed by slow isomerization of the EI complex to form the final complex EI*. To discriminate between the two mechanisms, the observed rate constant k_{obs} from the progress curve of the enzyme reaction is determined as a function of inhibitor concentration. A plot of k_{obs} versus inhibitor concentration is linear for mechanism A and hyperbolic for mechanism B.

Progress curves for efavirenz binding to p66^{W401A}, p51^{W401A}, and p66/p51 were measured at multiple inhibitor concentrations. Figure 4 shows the set of curves for p51^{W401A}. The solid lines are the fits to eq 2a to yield values of k_{obs}. Similar curves were obtained for p66^{W401A} and p66/p51. Figure 5 shows the plots of k_{obs} versus inhibitor concentration. The linear fits are consistent with mechanism A, where

$$k_{obs} = k_{-1} + k_1[I] \quad (3)$$

Values of the rate constants k_1 and k_{-1} calculated from the slopes and intercepts of Figure 5 are given in Table 2. All three proteins have similar association rate constants k_1 of ~13.5 M^{-1} s^{-1}. Additionally, the dissociation rate constants k_{-1} were 5.9−8.1 × 10^{-5} s^{-1}, corresponding to a $t_{1/2}$ of ~2.7 h. Having defined the binding modality of efavirenz, we calculated values of $K_d(3)^{app}$ from the ratio of k_{-1}/k_1.

The kinetics of dissociation of p66^{W401A}− and p51^{W401A}−EFV complexes were measured under essentially irreversible conditions, so that at equilibrium, <3% of the monomer−EFV complex is present (Figure 6). Dissociation rate constants k_{-1}(diss) of ~9.0 × 10^{-5} s^{-1} ($t_{1/2}$ ~ 2.1 h) were obtained for both monomers from fitting the data to eq 2b. The k_{-1}(diss) values from kinetics measurements are close to the k_{-1} values determined from the plots of k_{obs} versus [I] (Table 2). The equilibrium dissociation constants $K_d(3)$ of 6.6 μM calculated from the ratio of the rate constants k_{-1}(diss)/k_1 for binding to the monomer are 2.5-fold higher than the values determined by equilibrium dialysis.

Fluorescence Quantum Yields. Fluorescence quantum yields of dimerization-defective monomers and wild-type heterodimer were measured in the absence and presence of efavirenz. To measure the extent of quenching, most of the protein must be bound to efavirenz. The quantum yields of monomer−EFV complexes were measured on solutions containing 1 μM monomer and 30 μM efavirenz equilibrated for 30 h at 5 °C, giving 94% monomer−EFV complex. The quantum yields of p66^{W401A} and p51^{W401A} monomers are the same within error (Table 3). Efavirenz binding decreases the quantum yield of both monomers

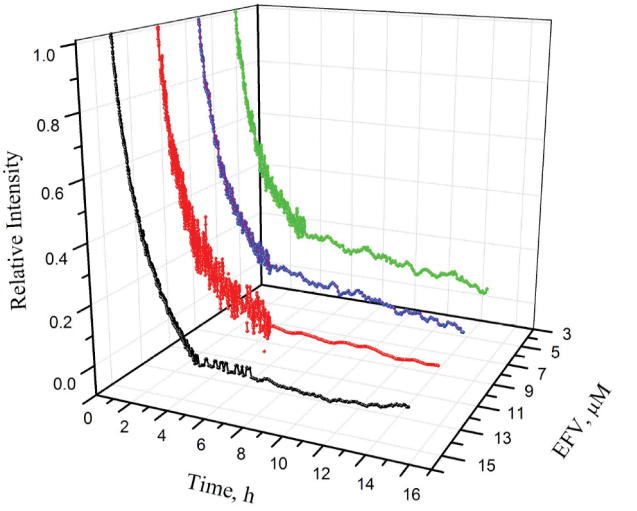

FIGURE 4: Progress curves for binding of p51^{W401A} to efavirenz monitored by tryptophan fluorescence at 5 °C. λ_{ex} = 295 nm, and λ_{em} = 340 nm: 2.5 μM p51^{W401A} with (green line) 5, (blue line) 8, (red line) 11, and (black line) 14 μM efavirenz. Data acquired at 30 s intervals for the first 4−5 h and then at 5 min intervals. Data were fit to eq 2a to yield k_{obs}.

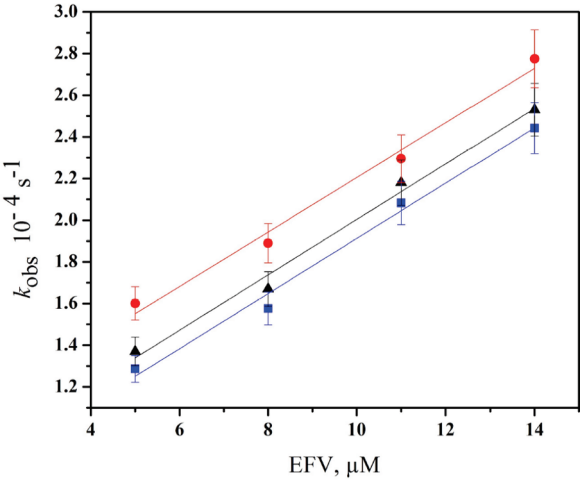

FIGURE 5: Progress curve analysis of binding of efavirenz to (▲) p66/p51, (red circles) p51^{W401A}, and (blue squares) p66^{W401A}. Lines are fits to eq 3. Error bars give the range of average values from two experiments.

Table 2: Kinetic Parameters[a]

protein	k_1[b] (M^{-1} s^{-1})	k_{-1}[b] (×10^{-5} s^{-1})	$K_d(3)^{app}$[c] (μM)	k_{-1}(diss)[d] (×10^{-5} s^{-1})
p51^{W401A}	13.7 ± 0.7	5.9 ± 0.7	4.2 ± 0.5	9.1 ± 0.2
p66^{W401A}	13.4 ± 0.6	8.1 ± 0.8	6.0 ± 0.3	8.9 ± 0.2
p66/p51	13.3 ± 0.9	6.7 ± 0.9	5.0 ± 0.3	nd

[a]RT buffer D, 1 mM TCEP, at 5 °C. [b]Calculated from eq 3 by linear regression of data in Figure 5. [c]$K_d(3)^{app} = k_{-1}/k_1$. [d]Calculated from eq 2b. Errors give the range of average values from two experiments.

by a factor of 3. To measure the quantum yield of the heterodimer, we diluted a 20 μM solution containing 83% dimer 50-fold and scanned it immediately as described above. The quantum yield of the heterodimer is approximately 25% lower than that of the monomers. The quantum yield of the p66/p51−EFV complex

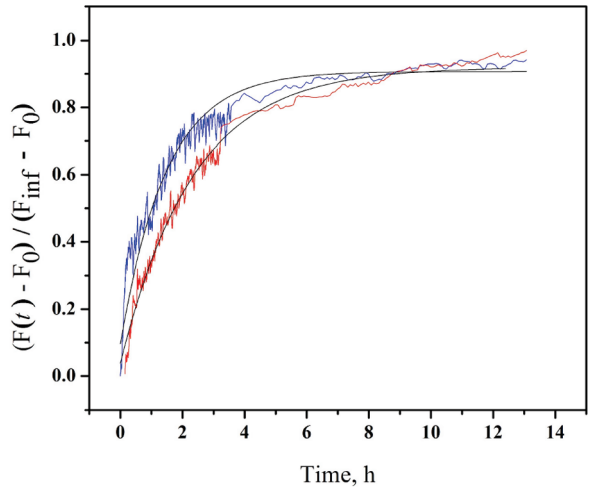

FIGURE 6: Dissociation of (red line) $p51^{W401A}$–EFV and (blue line) $p66^{W401A}$–EFV complexes monitored by tryptophan fluorescence at 5 °C. λ_{ex} = 295 nm, and λ_{em} = 340 nm. Black curves are fits to eq 2b. Data acquired at 30 s intervals for the first 4–5 h and then at 5 min intervals.

Table 3: Quantum Yields[a]

protein	Φ
$p51^{W401A}$	0.14 ± 0.01
$p51^{W401A}$–EFV complex	0.05 ± 0.02
$p66^{W401A}$	0.15 ± 0.01
$p66^{W401A}$–EFV complex	0.05 ± 0.02
p66/p51	0.11 ± 0.01
p66/p51–EFV complex	0.07 ± 0.01
NATA	0.23

[a]RT buffer D, 1 mM TCEP, at 5 °C. λ_{ex} = 295 nm. Errors are standard deviations of four experiments.

was measured in solutions containing 20 μM p66/p51 and 40 μM efavirenz equilibrated for 1 week at 5 °C prior to dilution. Because efavirenz enhances dimerization 25-fold and binds more tightly to the dimer than to the monomer, this solution contains 98% p66/p51–EFV complex. Efavirenz binding to heterodimer only quenches the fluorescence by a factor of 1.6.

Native Gel Electrophoresis. BN-PAGE has been used to monitor dimerization of RT proteins in the absence and presence of efavirenz (*21*). The slow dissociation rate of efavirenz ($t_{1/2} \sim 2$ h) makes it possible to visualize binding of [^{14}C]efavirenz to monomer on gels. $p66^{W401A}$ and wild-type p66 were incubated with a 0.7:1.0 ratio of [^{14}C]efavirenz to protein. The wild-type p66 concentration was 5 μM or approximately 53% homodimer. Lane 1 shows binding of [^{14}C]efavirenz to the $p66^{W401A}$ monomer. Lane 2 shows binding of [^{14}C]efavirenz to a mixture of wild-type p66 monomer and p66/p66 homodimer. Lastly, lane 3 shows enhancement of dimerization by efavirenz after equilibration of wild-type p66 with [^{14}C]efavirenz and excess cold efavirenz for 1 week, giving 91% p66/p66–EFV complex. Thus, BN-PAGE supports the conclusions from equilibrium dialysis that efavirenz binds to RT monomers as well as homodimers.

Nevirapine has been reported to have disparate effects on RT dimerization. Yeast two-hybrid experiments indicate a small enhancement of dimerization, whereas urea denaturation studies find no effect (*16*, *23*). BN-PAGE was performed using p66 incubated with excess efavirenz or nevirapine for 1 week. Figure 7B shows that both NNRTIs enhance dimerization, with

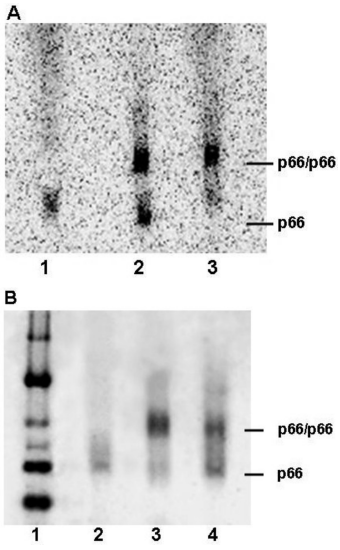

FIGURE 7: Blue Native polyacrylamide gel electrophoresis of p66 in the absence and presence of NNRTIs. (A) Monomer and homodimer binding to [^{14}C]EFV: (lane 1) 2 μM $p66^{W401A}$ incubated for 2 h with [^{14}C]EFV, (lane 2) 5 μM p66 incubated for 2 h with [^{14}C]EFV, and (lane 3) 5 μM p66 incubated for 1 week with [^{14}C]EFV. (B) Wild-type p66 incubated for 1 week in the absence and presence of NNRTI: (lane 1) native markers, (lane 2) 0.8 μM p66, (lane 3) 3 μM p66 and 25 μM EFV, and (lane 4) 3 μM p66 and 25 μM NVP.

efavirenz having the stronger effect. These results are consistent with the findings of the yeast two-hybrid experiments.

DISCUSSION

Although RT has been extensively studied for almost two decades, new functions continue to be discovered for this enigmatic enzyme. This paper reports two novel functions: (1) efavirenz, and presumably also other NNRTIs, binds to monomeric forms of RT, and (2) efavirenz is a slow binding inhibitor of monomers and heterodimer. The biological significance of monomer binding is unknown at present. NNRTIs have been found to affect both early and late stages of the HIV-1 replication cycle by multiple mechanisms (*31*, *32*). Efavirenz interacts at the level of reverse transcription by inhibiting DNA polymerase activity, enhancing polymerase-dependent RNase H activity (3′-DNA-directed), and partially inhibiting polymerase-independent RNase H activity (5′-RNA-directed). It also inhibits plus-strand initiation by affecting the ability of RT to bind the RNA polypurine tract. During late stages of HIV-1 replication, efavirenz enhances processing and homodimerization of a 90 kDa Pol polyprotein in a yeast two-hybrid system and enhances intracellular processing of Gag and Gag-Pol precursor polyproteins in HIV-1-transfected cells (*11*). By increasing the processing of these polyproteins, efavirenz lowers viral production due to decreased levels of full constructs for incorporation into a budding particle. Essential to the above processes is defining the binding properties of the species, whether monomer or dimer, to which efavirenz binds. Drug design requires an immense understanding of the target. This study suggests that monomeric forms of RT may be potential targets for HIV-1 therapeutics. It also sparks development of high-throughput screening assays based on p66 and p51 monomers in the evaluation of binding of new drugs to wild-type and drug resistance mutant RTs.

The two crystal structures of RT–EFV complexes show 1:1 binding stoichiometry (*9*, *33*). Currently, no crystal structures

are available for homodimers or monomers of RT. Equilibrium dialysis indicated a 1:1 stoichiometry for p66/p66− and p51/p51−EFV complexes. A 1:1 binding stoichiometry for monomer−EFV complexes was also obtained by equilibrium dialysis for wild-type p51 and dimerization-deficient $p66^{W401A}$ and $p51^{W401A}$, albeit with an affinity lower than that of the homodimers (Table 1). The apparent free energies of binding of efavirenz to homodimers at 5 °C ($\Delta G^{278} = -RT \ln K_a$) are −35.1 kJ/mol for the p66/p66−EFV complex and −43.6 kJ/mol for the p51/p51−EFV complex. The more favorable binding energy of the p51/p51 homodimer may be attributed to better contacts between efavirenz and the protein or more facile formation of the binding pocket in a dimer lacking two RNase H domains. All monomers have similar efavirenz binding energies ΔG^{278} of ∼ −30 kJ/mol, which is 5−12 kJ/mol less favorable than that for binding to homodimers.

The dissociation constants $K_d(1)$ and $K_d(3)$ from equilibrium dialysis (Table 1) and $K_d(2)$ and $K_d(4)$ from previous sedimentation equilibrium experiments allow us to complete the thermodynamic linkage of NNRTI binding and subunit dimerization proposed for RT (*14*). In the closed cycle of Scheme 1, $\Delta G = 0$. Substituting ΔG^{278} gives

$$-RT \ln K_a(2) - RT \ln K_a(3) = -RT \ln K_a(1) - RT \ln K_a(4) \quad (4)$$

In the case of p66, the left side of eq 4 sums to -68 ± 6 kJ/mol and the right side to -64 ± 4 kJ/mol. In the case of p51, the left side of eq 4 totals -64 ± 4 kJ/mol and the right side -63 ± 6 kJ/mol. These results for homodimers confirm the hypothesis that NNRTI binding is coupled to subunit dimerization. Thus, we can calculate the dissociation constant of the p66/p51−EFV complex $K_d(1)$ from the cycle in Scheme 1, where $K_d(2)$ and $K_d(4)$ are the dissociation constants of the heterodimer in the presence and absence of efavirenz (*14*), respectively, and $K_d(3)$ is the dissociation constant of the p66− or p51−EFV complex. Rearranging eq 4 gives $RT \ln K_a(1) = 38 \pm 6$ kJ/mol or $K_d(1) = 92 \pm 5$ nM. Most studies of binding of efavirenz to RT have employed polymerase activity assays, conducted in the presence of template/primer and dNTP (*12*, *34*, *35*). Maga et al. (*35*) reported a dissociation constant of 150 nM for the free RT−EFV complex extracted from enzymatic data. Geitmann et al. (*36*) measured binding of several NNRTIs to immobilized wild-type and drug resistance mutant RTs by SPR at 25 °C in buffer containing 0.005% surfactant and 3% (v/v) DMSO. An overall dissociation constant of 45 nM was obtained for binding of efavirenz to wild-type RT.

The binding kinetics monitored by tryptophan fluorescence establish that efavirenz is a slow, tight binding inhibitor of RT. Dissociation rate constants k_{-1}(diss) of 9.0×10^{-5} s^{-1} ($t_{1/2} = 2.1$ h) were obtained for monomer−EFV complexes. Association rate constants k_1 of 13.5 M^{-1} s^{-1} were obtained for the reversible, direct binding of efavirenz to both monomers and heterodimer (Scheme 2, mechanism A). This suggests that NNRTI binding occurs by an analogous process for monomeric and dimeric species of RT, despite the difference in efavirenz binding affinity. Slow binding inhibitors described in the literature follow either direct binding or conformational change inhibition models (Scheme 2). For example, small aza sugar inhibitors of β-glucosidase and yeast isomaltase bind by the direct mechanism A with association rate constants ranging from 23 to 7.3×10^4 M^{-1} s^{-1} (*37*). These inhibitors also have slow dissociation rate constants of $0.16-6.7 \times 10^{-2}$ s^{-1}. By contrast, peptide α-keto acid analogues are slow binding inhibitors of hepatitis C virus NS3 protease that bind by induced-fit mechanism B (*38*). These inhibitors undergo rapid equilibration with the enzyme in the first step of EI complex formation with a k_1 of 6.5×10^7 M^{-1} s^{-1} and a k_{-1} of 0.2 s^{-1}. The subsequent step is a slow isomerization to EI* with a k_2 of $1.7-7.5 \times 10^{-3}$ s^{-1} and a k_{-2} of $0.57-1.8 \times 10^{-5}$ s^{-1} or a $t_{1/2}$ of 11−48 h.

A few previous reports noted the slow onset of inhibition by NNRTIs. For example, 5−20 min preincubation periods of RT with NNRTIs were required to witness inhibition of polymerase and RNase H activity (*31*, *35*, *39*, *40*). The slow association rate constants reported here (Table 2) could be caused by a conformational selection step involving exclusive binding of a weakly populated conformer of either protein or inhibitor. The chemical structure of efavirenz is provided in Figure 2. The benzoxazinone ring system is rigid with free rotation of the cyclopropyl ethynyl group (*41*). Efavirenz is in the same position in the binding pocket in both crystal structures of the wild-type RT−EFV complex. However, the cyclopropyl ethynyl group is rotated ∼100° in the drug resistance mutant K103N RT−EFV complex relative to the position in the wild-type structures (*9*, *33*). The rigidity of the efavirenz core together with the ability of the binding pocket to accommodate different orientations of the cyclopropyl ethynyl group excludes conformational selection of the inhibitor as the culprit.

A selected-fit model has been proposed in which a conformational pre-equilibration of the protein precedes inhibitor binding (*36*, *42*). In this model for slow binding, efavirenz would bind preferentially to a less populated conformer of RT proteins. Productive collisions occurring between inhibitor and this conformer would induce a slow shift in the conformational equilibrium favoring formation of the binding pocket and subsequently the EI complex. A less likely alternative would be severe orientation effects resulting in unproductive collisions of E and I that slow formation of the EI complex in the direct binding mechanism A. A selected-fit model gave the best fit to the SPR data for wild-type RT and efavirenz with an overall association rate constant k_{on} of 5.5×10^4 M^{-1} s^{-1}. This k_{on} value is 3 orders of magnitude faster then our association rate constant k_1 for binding of efavirenz to p66/p51. The dissociation rate constant k_{off} of $\sim 2.3 \times 10^{-3}$ s^{-1} is ∼20-fold faster then the k_{-1} value obtained from progress curve analysis. A probable explanation for the faster binding kinetics is the different solution conditions used in the SPR assay. Osmolytes such as detergents, organic solvents, and salts affect protein solution structure and interactions (*43*, *44*).

The NNRTI binding pocket is absent from structures of RT and RT−substrate complexes (*45*, *46*). The polymerase domain is composed of four subdomains: fingers, palm, thumb, and connection. The structure of RT is asymmetric, and the subdomains are in different orientations in the p66 and p51 subunits [Figure 8, top (*45*)]. In RT−NNRTI complexes, the binding pocket is in the palm of the p66 subunit of the heterodimer [Figure 8, bottom (*9*)]. LPC software identifies 14 residues that contact efavirenz in the NNRTI binding pocket of the p66 subunit: L100, K101, K103, V106, V179, Y181, Y188, G190, F227, W229, L234, H235, P236, and Y318 (*47*). The efavirenz contact residues are highlighted in Figure 8 to illustrate the location of these residues in the two subunits. Although the contact residues are clustered in both subunits, these residues do not form a binding pocket in the p51 subunit. The p66/p66 and p51/p51 homodimers may also have

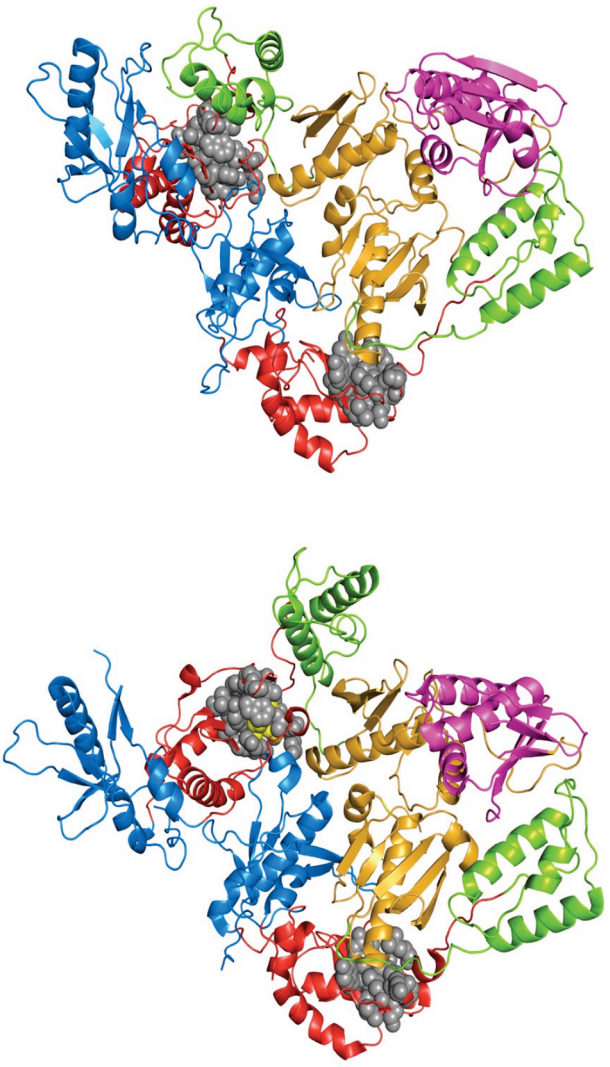

FIGURE 8: Structures of HIV-1 (top) RT (PDB entry 1DLO) and (bottom) the RT−EFV complex (PDB entry 1FK9). Polymerase domains: fingers (blue), palm (red), thumb (green), and connection (orange) subdomains; RNase H domain (magenta). Efavirenz (yellow) and contact residues (gray) are shown using the van der Waals radii.

asymmetric structures, because they both have polymerase activity (*3*). Additionally, the homodimers probably have similar NNRTI binding pockets in the subunit that binds the inhibitor, because p66 and p51 have identical amino acid sequences and similar folding patterns of the polymerase subdomains. Given that p66 and p51 monomers are capable of forming a competent NNRTI binding pocket, presumably the polymerase domain of both monomers must adopt a conformation analogous to that of the p66 subunit in the heterodimer.

ACKNOWLEDGMENT

We are grateful to Ms. Kathryn J. Howard for suggesting the gel experiment with [^{14}C]efavirenz and for advice about site-directed mutagenesis and protein purification. We also thank Dr. Clare Woodward for suggesting that NNRTIs bind to monomers and Drs. Vernon Anderson and Jonathan Karn for helpful discussions.

APPENDIX

Dialfit: Mathematical Models and Data Analysis (by Leslie A. Holladay).

There are two different ways in which the model equations may be written: case A and case B.

Case A. For case A, the following equilibrium constants are defined as

$$\mathrm{P}+\mathrm{I}=\mathrm{PI} \quad K_a(3)=[\mathrm{PI}]/([\mathrm{P}][\mathrm{I}]) \tag{A1a}$$

$$\mathrm{P}+\mathrm{P}=\mathrm{PP} \quad K_a(4)=[\mathrm{PP}]/[\mathrm{P}]^2 \tag{A1b}$$

$$\mathrm{PP}+\mathrm{I}=\mathrm{PPI} \quad K_a(1)=[\mathrm{PPI}]/([\mathrm{PP}][\mathrm{I}]) \tag{A1c}$$

The equilibrium dialysis experiment involves computing the total molar concentration of inhibitor bound to both monomer and dimer $[I_{bound}]$, by subtracting the concentration of free inhibitor outside the dialysis bag $[I_{out}] = [I]$ from the total concentration of inhibitor inside the bag $[I_{in}]$ as in eq 1. For the data analysis, the observable variable we wish to model is $[I_{bound}]$. The total concentration of protein $[P]_{tot}$ inside the bag is presumed to be known to higher precision than the free and bound inhibitor concentrations. $[I_{bound}]$ is the observable to be predicted knowing [I] and $[P]_{tot}$ along with the current estimates for $K_a(1)$, $K_a(3)$, and $K_a(4)$. Dialfit is applicable to any experiment that provides data for $[I_{bound}]$ and [I], knowing $[P]_{tot}$.

To compute $[I_{bound}]$, the concentration of free protein monomer [P] must first be computed. The conservation of mass equation is

$$[\mathrm{P}]_{tot}=[\mathrm{P}]+[\mathrm{PI}]+2[\mathrm{PP}]+2[\mathrm{PPI}] \tag{A2}$$

Rearranging and substituting terms with the equilibrium constants from eqs A1 result in a quadratic in [P]

$$a[\mathrm{P}]^2+b[\mathrm{P}]+c=0 \tag{A3a}$$

where

$$a=2K_a(4)+2K_a(1)K_a(4)[\mathrm{I}] \tag{A3b}$$

$$b=1+K_a(3)[\mathrm{I}] \tag{A3c}$$

$$c=-[\mathrm{P}]_{tot} \tag{A3d}$$

The only physical meaningful root of eq A3a is the positive one. The fitting function may be written as

$$[I_{bound}]=K_a(3)[\mathrm{P}][\mathrm{I}]+K_a(1)K_a(4)[\mathrm{P}]^2[\mathrm{I}] \tag{A4}$$

The values of $[I_{bound}]$ determined over a wide range of total inhibitor and total protein concentrations are globally fitted to eq A4. Note that $K_a(1)$ and $K_a(4)$ cannot be separated, and thus, one value must be a fixed parameter.

Case B. For case B, two equilibrium constants are defined in eqs A1a and A1b; the third equilibrium constant is defined as

$$\mathrm{PI}+\mathrm{P}=\mathrm{PPI} \quad K_a(2)=[\mathrm{PPI}]/([\mathrm{PI}][\mathrm{P}]) \tag{A5}$$

Here too, $[I_{bound}]$ is the observable to be predicted knowing [I] and $[P]_{tot}$, but with the current estimates for $K_a(2)$, $K_a(3)$, and $K_a(4)$. The conservation of mass equation A2 and quadratic equations A3a, A3c, and A3d are the same as in case A; eq A3b becomes

$$a=2K_a(4)+2K_a(2)K_a(3)[\mathrm{I}] \tag{A6}$$

Again, the physically meaningful root of eq A3a is the positive one. The fitting function is

$$[I_{bound}]=K_a(3)[\mathrm{P}][\mathrm{I}]+K_a(2)K_a(3)[\mathrm{P}]^2[\mathrm{I}] \tag{A7}$$

Note that cases A and B are mathematically equivalent from the

relationship $K_a(1)K_a(4) = K_a(2)K_a(3)$. The two parameters $K_a(2)$ and $K_a(3)$ are not separable, and thus, the value of $K_a(2)$ must be fixed.

Weighted Least-Squares and Parameter Standard Errors. The global data sets have a very wide range of values for $[I_{bound}]$ and [I]. For radioactive counts, the relative standard deviation is equal to $\sqrt{N}/N$, where N is the number of counts (*48*). The relative variance is equal to $1/N$. $[I_{bound}]$ is computed from the difference in counts inside and outside the bag. Define the number of counts inside the bag as N_i and the number of counts outside the bag as N_o. Then the relative variance of the difference $N_i - N_o = (N_i + N_o)/(N_iN_o)$. In the situation in which the values for $[I_{bound}]$ and [I] vary over several orders of magnitude, it is essential to use weighted least squares because the variance will also vary over a wide range (*49*). The weight W_j of any $(N_i - N_o)_j$ value is the reciprocal of the variance, so $W_j = [(N_iN_o)/(N_i + N_o)]_j$. The actual weights used are normalized so that the $\Sigma_j W_j = 1$ to cause the returned residual error in the fit to be correct. It is clear from Figure 1 (insets) that the errors in $[I_{bound}]$ are very heteroscedastic. The errors in the fitted variable vary greatly with respect to the independent variable. Only if the errors are homoscedastic is unweighted least squares appropriate.

Standard errors for the parameter values were computed using the "balanced bootstrap" with 100 trials (*50*, *51*). If any of the individual bootstrap trials was more than three standard deviations away from the parameter estimate, that trial was deleted as an outlier and the standard deviation recomputed. The 95% confidence intervals are computed using the standard deviation from the estimated parameter value.

REFERENCES

1. di Marzo Veronese, F., Copeland, T. D., DeVico, A. L., Rahman, R., Oroszlan, S., Gallo, R. C., and Sarngadharan, M. G. (1986) Characterization of highly immunogenic p66/p51 as the reverse transcriptase of HTLV-III/LAV. *Science 231*, 1289–1291.
2. Hizi, A., McGill, C., and Hughes, S. H. (1988) Expression of soluble, enzymatically active, human immunodeficiency virus reverse transcriptase in *Escherichia coli* and analysis of mutants. *Proc. Natl. Acad. Sci. U.S.A. 85*, 1218–1222.
3. Restle, T., Müller, B., and Goody, R. S. (1990) Dimerization of human immunodeficiency virus type 1 reverse transcriptase. *J. Biol. Chem. 265*, 8986–8988.
4. Restle, T., Müller, B., and Goody, R. S. (1992) RNase H activity of HIV reverse transcriptase is confined exclusively to the dimeric forms. *FEBS Lett. 300*, 97–100.
5. Le Grice, S. F. J., Naas, T., Wohlgensinger, B., and Schatz, O. (1991) Subunit-selective mutagenesis indicates minimal polymerase activity in heterodimer-associated p51 HIV-1 reverse transcriptase. *EMBO J. 10*, 3905–3911.
6. Tsai, C. H., Lee, P. Y., Stollar, V., and Li, M. L. (2006) Antiviral therapy targeting viral polymerase. *Curr. Pharm. Des. 12*, 1339–1355.
7. De Clercq, E. (1998) The role of non-nucleoside reverse transcriptase inhibitors (NNRTIs) in the therapy of HIV-1 infection. *Antiviral Res. 38*, 153–179.
8. Kohlstaedt, L. A., Wang, J., Friedman, J. M., Rice, P. A., and Steitz, T. A. (1992) Crystal structure at 3.5 Å resolution of HIV-1 reverse transcriptase complexed with an inhibitor. *Science 256*, 1783–1790.
9. Ren, J., Milton, J., Weaver, K. L., Short, S. A., Stuart, D. I., and Stammers, D. K. (2000) Structural basis for the resilience of efavirenz (DMP-266) to drug resistance mutations in HIV-1 reverse transcriptase. *Structure 8*, 1089–1094.
10. Merluzzi, V. J., Hargrave, K. D., Labadia, M., Grozinger, K., Skoog, M., Wu, J. C., Shih, C.-K., Eckner, K., Hattox, S., Adams, J., Rosenthal, A. S., Faanes, R., Eckner, R. J., Koup, R. A., and Sutton, J. L. (1990) Inhibition of HIV-1 replication by a nonnucleoside reverse transcriptase inhibitor. *Science 250*, 1411–1413.
11. Figueiredo, A., Moore, K. L., Mak, J., Sluis-Cremer, N., de Bethune, M.-P., and Tachedjian, G. (2006) Potent nonnucleoside reverse transcriptase inhibitors target HIV-1 Gag-Pol. *PLoS Pathog. 2*, 1051–1059.
12. Young, S. D., Britcher, S. F., Tran, L. O., Payne, L. S., Lumma, W. C., Lyle, T. A., Huff, J. R., Anderson, P. S., Olsen, D. B., Carroll, S. S., Pettibone, D. J., O'Brien, J. A., Ball, R. G., Balani, S. K., Lin, J. H., Chen, I.-W., Schleif, S. A., Sardana, V. V., Long, W. J., Byrnes, V. W., and Emini, E. A. (1995) L-743,726 (DMP-266): A novel, highly potent nonnucleoside inhibitor of the human immunodeficiency virus type 1 reverse transcriptase. *Antimicrob. Agents Chemother. 39*, 2602–2605.
13. Tachedjian, G., Orlova, M., Sarafianos, S. G., Arnold, E., and Goff, S. P. (2001) Nonnucleoside reverse transcriptase inhibitors are chemical enhancers of dimerization of the HIV type 1 reverse transcriptase. *Proc. Natl. Acad. Sci. U.S.A. 98*, 7188–7193.
14. Venezia, C. F., Howard, K. J., Ignatov, M. E., Holladay, L. A., and Barkley, M. D. (2006) Effects of efavirenz binding on the subunit equilibria of HIV-1 reverse transcriptase. *Biochemistry 45*, 2779–2789.
15. Sluis-Cremer, N., Arion, D., and Parniak, M. A. (2002) Destabilization of the HIV-1 reverse transcriptase dimer upon interaction with *N*-acyl hydrazone inhibitors. *Mol. Pharmacol. 62*, 398–405.
16. Sluis-Cremer, N., Dmitrienko, G. I., Balzarini, J., Camarasa, M.-J., and Parniak, M. A. (2000) Human immunodeficiency virus type 1 reverse transcriptase dimer destablilization by 1-{spiro[4″-amino-2″,2″-dioxo-1″,2″-oxathiole-5″,3′-[2′,5′-bis-*O*-(*tert*-butyldimethylsilyl)-β-D-ribofuranosyl]]}-3-ethylthymine. *Biochemistry 39*, 1427–1433.
17. Le Grice, S. F. J., Cameron, C. E., and Benkovic, S. J. (1995) Purification and characterization of human immunodeficiency virus type 1 reverse transcriptase. *Methods Enzymol. 262*, 130–144.
18. Ignatov, M. E., Berdis, A. J., Le Grice, S. F. J., and Barkley, M. D. (2005) Attenuation of DNA replication by HIV-1 reverse transcriptase near the central termination sequence. *Biochemistry 44*, 5346–5356.
19. Tachedjian, G., Aronson, H.-E., de los Santos, M., Seehra, J., McCoy, J. M., and Goff, S. P. (2003) Role of residues in the tryptophan repeat motif for HIV-1 reverse transcriptase dimerization. *J. Mol. Biol. 326*, 381–396.
20. Chen, R. F. (1967) Fluorescence quantum yields of tryptophan and tyrosine. *Anal. Lett. 1*, 35–42.
21. Braz, V. A., and Howard, K. J. (2009) Separation of protein oligomers by blue native gel electrophoresis. *Anal. Biochem. 388*, 170–172.
22. Ghosh, M., Jacques, P. S., Rodgers, D. W., Ottman, M., Darlix, J. L., and Le Grice, S. F. J. (1996) Alterations to the primer grip of p66 HIV-1 reverse transcriptase and their consequences for template-primer utilization. *Biochemistry 35*, 8553–8562.
23. Tachedjian, G., Aronson, H.-E. G., and Goff, S. P. (2000) Analysis of mutations and suppressors affecting interactions between subunits of the HIV type 1 reverse transcriptase. *Proc. Natl. Acad. Sci. U.S.A. 97*, 6334–6339.
24. Vivian, J. T., and Callis, P. R. (2001) Mechanisms of tryptophan fluorescence shifts in proteins. *Biophys. J. 80*, 2093–2109.
25. Callis, P. R., Petrenko, A., Muiño, P. L., and Tusell, J. R. (2007) Ab initio prediction of tryptophan fluorescence quenching by protein electric field enabled electron transfer. *J. Phys. Chem. B 111*, 10335–10339.
26. Divita, G., Restle, T., and Goody, R. S. (1993) Characterization of the dimerization process of HIV-1 reverse transcriptase heterodimer using intrinsic protein fluorescence. *FEBS Lett. 324*, 153–158.
27. Barnard, J., Borkow, G., and Parniak, M. A. (1997) The thiocarboxanilide nonnucleoside UC781 is a tight-binding inhibitor of HIV-1 reverse transcriptase. *Biochemistry 36*, 7786–7792.
28. Venezia, C. F., Meany, B. J., Braz, V. A., and Barkley, M. D. (2009) Kinetics of association and dissociation of HIV-1 reverse transciptase subunits. *Biochemistry 48*, 9084–9093.
29. Copeland, R. A. (2005) Evaluation of Enzyme Inhibitors in Drug Discovery, John Wiley & Sons, New York.
30. Szedlacsek, S. E., and Duggleby, R. G. (1995) Kinetics of slow and tight-binding inhibitors. *Methods Enzymol. 249*, 144–180.
31. Sluis-Cremer, N., and Tachedjian, G. (2008) Mechanisms of inhibition of HIV replication by non-nucleoside reverse transcriptase inhibitors. *Virus Res. 134*, 147–156.
32. Grobler, J. A., Dornadula, G., Rice, M. R., Simcoe, A. L., Hazuda, D. J., and Miller, M. D. (2007) HIV-1 reverse transcriptase plus-strand initiation exhibits preferential sensitivity to non-nucleoside reverse transcriptase inhibitors in vitro. *J. Biol. Chem. 282*, 8005–8010.
33. Lindberg, J., Sigurdsson, S., Löwgren, S., Andersson, H. O., Sahlberg, C., Noréen, R., Fridborg, K., Zhang, H., and Unge, T. (2002) Structural basis for the inhibitory efficacy of efavirenz (DMP-266), MSC194 and PNU142721 towards the HIV-1 RT K103N mutant. *Eur. J. Biochem. 269*, 1670–1677.
34. Xia, Q., Radzio, J., Anderson, K. S., and Sluis-Cremer, N. (2007) Probing nonnucleoside inhibitor-induced active site distortion in

HIV-1 reverse transcriptase by transient kinetics analysis. *Protein Sci. 16*, 1728–1737.
35. Maga, G., Ubiali, D., Salvetti, R., Pregnolato, M., and Spadari, S. (2000) Selective interaction of the human immunodeficiency virus type 1 reverse transcriptase nonnucleoside inhibitor efavirenz and its thio-substituted analog with different enzyme-substrate complexes. *Antimicrob. Agents Chemother. 44*, 1186–1194.
36. Geitmann, M., Unge, T., and Danielson, H. (2006) Interaction kinetic characterization of HIV-1 reverse transcriptase non-nucleoside inhibitor resistance. *J. Med. Chem. 49*, 2375–2387.
37. Lohse, A., Hardlei, T., Jensen, A., Plesner, I. W., and Bols, M. (2000) Investigation of the slow inhibition of almond β-glucosidase and yeast isomaltase by 1-azasugar inhibitors: Evidence for the 'direct binding' model. *Biochem. J. 349*, 211–215.
38. Narjes, F., Brunetti, M., Colarusso, S., Gerlach, B., Koch, U., Biasiol, G., Fattori, D., De Francesco, R., Matassa, V. G., and Steinkühler, C. (2000) α-Ketoacids are potent slow binding inhibitors of the hepatitis C virus NS3 protease. *Biochemistry 39*, 1849–1861.
39. Borkow, G., Fletcher, R. S., Barnard, J., Arion, D., Motakis, D., Dmitrienko, G. I., and Parniak, M. A. (1997) Inhibition of the ribonuclease H and DNA polymerase activities of HIV-1 reverse transcriptase by *N*-(4-*tert*-butylbenzoyl)-2-hydroxy-1-napthaldehyde hydrazone. *Biochemistry 36*, 3179–3185.
40. Spence, R. A., Kati, W. M., Anderson, K. S., and Johnson, K. A. (1995) Mechanism of inhibition of HIV-1 reverse transcriptase by nonnucleoside inhibitors. *Science 267*, 988–993.
41. Wang, D.-E., Rizzo, R. C., Tirado-Rives, J., and Jorgensen, W. L. (2001) Antiviral drug design: Computational analyses of the effects of the L100I mutation for HIV-RT on the binding of NNRTIs. *Bioorg. Med. Chem. Lett. 11*, 2799–2802.
42. Weikl, T. R., and von Deuster, C. (2009) Selected-fit versus induced-fit protein binding: Kinetic differences and mutational analysis. *Proteins 75*, 104–110.
43. Pegram, L. M., and Record, M. T., Jr. (2008) Thermodynamic origin of Hofmeister ion effects. *J. Phys. Chem. B 112*, 9428–9436.
44. Rösgen, J., Pettitt, B. M., and Bolen, D. W. (2005) Protein folding, stability, and solvation structure in osmolyte solutions. *Biophys. J. 89*, 2988–2997.
45. Hsiou, Y., Ding, J., Das, K., Clark, A. D., Jr., Hughes, S. H., and Arnold, E. (1996) Structure of unliganded HIV-1 reverse transcriptase at 2.7 Å resolution: Implications of conformational changes for polymerization and inhibition mechanism. *Structure 4*, 853–860.
46. Huang, H., Chopra, R., Verdine, G. L., and Harrison, S. C. (1998) Structure of a covalently trapped catalytic complex of HIV-1 reverse transcriptase: Implications for drug resistance. *Science 282*, 1669–1675.
47. Sobolev, V., Sorokine, A., Prilusky, J., Abola, E. E., and Edelman, M. (1999) Automated analysis of interatomic contacts in proteins. *Bioinformatics 15*, 327–332.
48. Willard, H. H., Merritt, L. L., Jr., and Dean, J. A. (1965) Instrumental Methods of Analysis, Vol. 256, D. Van Nostrand Company, New York.
49. Draper, N. R., and Smith, H. (1966) Applied Regression Analysis, pp 77−81, Wiley & Sons, New York.
50. Efron, B., and Tibshrirani, R. (1986) Bootstrap methods for standards errors, confidence intervals, and other measures of statistical accuracy. *Stat. Sci. 1*, 54–77.
51. Hall, P. (1992) The Bootstrap and Edgeworth Expansion, p 293, Springer-Verlag, New York.